Spectroscopy and Photophysics of $Rh_2(dimen)_4^{2+}$ (dimen = 1,8-Diisocyanomenthane). Exceptional Metal–Metal Bond Shortening in the Lowest Electronic Excited States

Vincent M. Miskowski,* Steven F. Rice, and Harry B. Gray*

Arthur Amos Noyes Laboratory, California Institute of Technology, Pasadena, California 91125

Richard F. Dallinger

Department of Chemistry, Wabash College, Crawfordsville, Indiana 47933

Steven J. Milder†

Department of Chemistry, Brookhaven National Laboratory, Upton, New York 11973

Michael G. Hill, Christopher L. Exstrom, and Kent R. Mann*

Department of Chemistry, University of Minnesota, Minneapolis, Minnesota 55455

Received October 22, 1993⊛

$Rh_2(dimen)_4^{2+}$ (dimen = 1,8-diisocyanomenthane) exhibits very long Rh–Rh bond distances in the solid state (varying from 4.48 Å for the PF_6^- salt to 3.861 Å for the $B(C_6H_5)_4^-$ salt), but the lowest $d\sigma^* \rightarrow p\sigma$ excitation produces an excited state with a considerably shorter Rh–Rh distance (~3.2 Å). Several techniques (absorption, single-crystal polarized absorption, emission, polarized excitation, resonance Raman, fluorescence, phosphorescence lifetime data, and MM2 calculations) help describe the ground- and lowest excited-state potential energy surfaces of this complex. The absorption corresponding to $d\sigma^* \rightarrow p\sigma$ singlet–singlet excitation ($^1A_{1g} \rightarrow {}^1A_{2u}$) is markedly asymmetric, with a sharp maximum (420–440 nm) and a long tailing shoulder (~480 nm). A similarly asymmetric $d\sigma^* \rightarrow p\sigma$ singlet–triplet feature ($^1A_{1g} \rightarrow {}^3A_{2u}$) is observed ~3000 cm^{-1} below the singlet–singlet band in the polarized single-crystal spectra of the $B(C_6H_5)_4^-$ salt. In contrast, the corresponding emission bands (545–600 nm, fluorescence; 660–714 nm, phosphorescence) are nearly symmetric. The spectroscopic properties are interpreted in terms of ground- and excited-state potential surfaces that combine parameters derived from previous work on more conventional $(Rh^I)_2$ systems with the results of MM2 calculations of dimen deformations. The calculated ground-state surface is very shallow, with a minimum at 4.75 Å, but nearly harmonic in the range of interest. The calculated excited-state surface is extremely anharmonic: after a well-defined minimum at 3.35 Å, it is broad and shallow at longer Rh–Rh distances. For Rh–Rh distances greater than ~4 Å, the calculations predict that the individual Rh(I) square planes of $Rh_2(dimen)_4^{2+}$ will be eclipsed; at shorter distances, these units are expected to twist (at a dihedral angle inversely proportional to the Rh–Rh separation) to relieve the substantial strain energy involved in distorting $Rh_2(dimen)_4^{2+}$ along the square planar, a_{2u} bending coordinate. These predictions are consistent with the crystal structures of $[Rh_2(dimen)_4][PF_6]_2$ (Rh–Rh = 4.48 Å; dihedral twist angle = 0°) and $[Rh_2(dimen)_4][B(C_6H_5)_4]_2$ (Rh–Rh = 3.861 Å; dihedral twist angle = 16.2°) and provide an explanation for the dramatic rigidochromic effect (1000-cm^{-1} blue shift) on the emission as the temperature is lowered through the glass transition of solutions.

Binuclear rhodium(I) complexes are characterized by weak ground-state metal–metal interactions (metal–metal bond lengths generally are near 3.2 Å) and electronic spectra that are strongly perturbed relative to those of mononuclear species.[1-3] An especially interesting case is $Rh_2(dimen)_4^{2+}$ (dimen = 1,8-diisocyanomethane),[4] which exhibits exceptionally long Rh–Rh distances in various salts (4.48 Å, PF_6^-;[4a] 4.246 Å, TFPB$^-$,[4b] where TFPB$^-$ = tetrakis[3,5-bis(trifluoromethyl)phenyl]borate; 3.861 Å, $B(C_6H_5)_4^-$ [4b]). Although the cyclohexyl moiety is relatively rigid (apparently disfavoring short metal–metal distances in d^8–d^8 and d^{10}–d^{10} systems),[4,5] the structure of $Rh_2(dimen)_2(dppm)_2^{2+}$ (dppm = bis(diphenylphosphino)methane) (Rh–Rh = 3.161 Å) shows that dimen is flexible enough to accommodate metal–

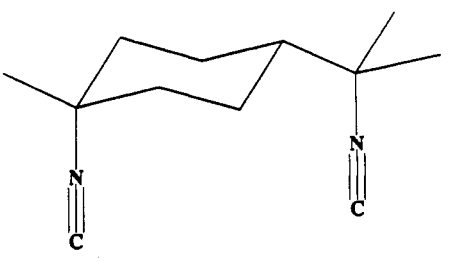

dimen

† Deceased December 23, 1993.

⊛ Abstract published in *Advance ACS Abstracts,* May 15, 1994.

(1) Miskowski, V. M.; Rice, S. F.; Gray, H. B.; Milder, S. J. *J. Phys. Chem.* **1993**, *97*, 4277–4283.

(2) Miskowski, V. M.; Nobinger, G. L.; Kliger, D. S.; Hammond, G. S.; Lewis, N. S.; Mann, K. R.; Gray, H. B. *J. Am. Chem. Soc.* **1978**, *100*, 485–488.

(3) Rice, S. F.; Miskowski, V. M.; Gray, H. B. *Inorg. Chem.* **1988**, *27*, 4704–4708.

(4) (a) Rhodes, M. R.; Mann, K. R. *Inorg. Chem.* **1984**, *23*, 2053–2058. (b) Hill, M. G.; Mann, K. R.; Miskowski, V. M.; Schaefer, W. P.; Gray, H. B. Unpublished work.

(5) (a) Gladfelter, W. L.; Gray, H. B. *J. Am. Chem. Soc.* **1980**, *102*, 5909–5910. (b) Che, C.-M.; Herbstein, F. H.; Schaefer, W. P.; Marsh, R. E.; Gray, H. B. *Inorg. Chem.* **1984**, *23*, 2572–2575. (c) Perrault, D.; Drouin, M.; Michael, A.; Harvey, P. D. *Inorg. Chem.* **1991**, *30*, 2–4. (d) Che, C.-M.; Yip, H.-K.; Wong, W.-T.; Lai, T.-F. *Inorg. Chim. Acta* **1992**, *197*, 177–183.

0020-1669/94/1333-2799$04.50/0

metal distances in the ~3-Å range.[6] For $Rh_2(dimen)_2(dppm)_2^{2+}$, the small bridging bite of the dppm ligands, in combination with the weak metal–metal bond, predominates over the dimen ligand constraint that favors a longer metal–metal distance. Additional examples include $[Ir_2(dimen)_4(P(C_6H_5)_3)(AuP(C_6H_5)_3)][PF_6]_3$[7a] and $[AgIr_2(dimen)_4(L)_2][PF_6]_3$ (L = $P(C_6H_5)_3$[7b] and dimethyl sulfoxide[7c]), where the Ir–Ir distances are 2.986 and 5.28 Å: the former complex exhibits a normal[8] d^7–d^7 single-bond distance, but an encapsulated Ag^+ ion forces a very large dimen bridging distance in the latter compound.[7c]

Further evidence of dimen flexibility comes from the spectroscopy of the 2e⁻-oxidized d^7–d^7 complex $Rh_2(dimen)_4Cl_2^{2+}$.[4] The electronic absorption spectrum of $Rh_2(dimen)_4Cl_2^{2+}$ exhibits a very intense $d\sigma \rightarrow d\sigma^*$ absorption at 337 nm (ϵ = 55 000 M^{-1} cm^{-1}), which is nearly identical with that seen for analogous d^7–d^7 compounds such as $Rh_2b_4Cl_2^{2+}$ and $Rh_2(TMB)_4Cl_2^{2+}$ (b = 1,3-diisocyanopropane; TMB = 2,5-dimethyl-2,5-diisocyanohexane).[8] These spectroscopic data strongly suggest that the Rh–Rh distances are similar in all of these d^7–d^7 complexes (~2.8 Å)[9] and that the formation of an axially ligated metal–metal single bond provides the driving force that overcomes the dimen ligand potential.[10]

The impressive range of metal–metal distances spanned by the dimen ligand suggests the possibility of unusual photophysical effects. The Rh–Rh bond strength in the ground state of binuclear d^8–d^8 complexes has been estimated to be about 12 kcal/mol[3,11] (roughly the same energy as the cyclohexane inversion barrier); thus, the ligand potential required to impose the long Rh–Rh distance in $Rh_2(dimen)_4^{2+}$ need not be very substantial. Indeed, the range of metal–metal distances measured for the PF_6^-, TFPB⁻, and $B(C_6H_5)_4^-$ salts of $Rh_2(dimen)_4^{2+}$ indicates that crystal packing forces are sufficient to perturb the equilibrium geometry of dimen-bridged species. Since states that arise from the $d\sigma^* \rightarrow p\sigma$ transition possess relatively strong Rh–Rh bonds (~36 kcal/mol),[3,11] the electronically excited Rh(I)–dimen complex could have a Rh–Rh distance near the 2.93 Å inferred for the $^3(d\sigma^* \rightarrow p\sigma)$ state of $Rh_2b_4^{2+}$.[3,12] As reported here, the results of extensive spectroscopic and photophysical measurements on $Rh_2(dimen)_4^{2+}$ demonstrate that a large excited-state Rh–Rh contraction does in fact occur.

Experimental Section

The compound $[Rh_2(dimen)_4][PF_6]_2$ was synthesized following a published method,[4a] and the $CF_3SO_3^-$, $B(C_6H_5)_4^-$, and TFPB⁻ (TFPB⁻ = tetrakis[3,5-bis(trifluoromethyl)phenyl]borate) salts were prepared by analogous procedures. Satisfactory elemental analyses were obtained. Solutions of these complexes were not air- or light-sensitive. Large crystals of $[Rh_2(dimen)_4][B(C_6H_5)_4]_2$ were grown by slow evaporation of concentrated acetonitrile/water solutions. Well-developed specimens were obtained as thin orange blades. The cell dimensions (orthorhombic, *Pbca*) were determined for a typical crystal on an X-ray diffractometer and were found to be identical with those of the crystal (obtained from acetonitrile/diethyl ether) that was used in an X-ray structure determination.[4b] The well-developed crystal face was identified as (001), and the axis orientations were also determined on the diffractometer. Samples dissolved in poly(methyl methacrylate) (PMMA) were obtained by slow evaporation of concentrated CH_2Cl_2 solutions of PMMA containing small amounts of $[Rh_2(dimen)_4][PF_6]_2$.

Diffuse reflectance spectra were measured on a home-built instrument in the laboratory of G. R. Rossman at Caltech. Emission and emission excitation spectra were obtained with a Perkin-Elmer MPF-66 spectrofluorimeter and were computer-corrected for instrumental factors.[13] Excitation spectra were determined for optically dilute (absorbance <0.1/cm) solutions. Polarized excitation spectra employed Glan-Thompson air-spaced calcite polarizers mounted in rotatable stages in front of the emission and excitation slits (90° geometry) of the spectrometer. For most runs, a polarization scrambler was placed between the emission slit and emission polarizer. Data were collected as four digital data files corresponding to the excitation spectra for the four possible combinations of vertical (v) or horizontal (h) polarizer orientations. The polarization ratio N for a particular wavelength is given by eq 1, where the first index

$$N = \frac{I_{vv}}{I_{vh}}\left(\frac{I_{hb}}{I_{hv}}\right) \quad (1)$$

on the intensities represents the excitation polarizer orientation and the second the emission polarizer orientation. The term in parentheses, which corrects for instrumental factors, equals 1 for an ideal spectrometer. Experimentally, we have found that this term is near unity and is independent of wavelength over the 230–600-nm range of our spectrometer.[13] We therefore present polarized excitation spectra as "corrected" $I_\parallel$ and $I_\perp$, where $I_\parallel = I_{vv}(I_{hh}/I_{hv})$ and $I_\perp = I_{vh}$.

The absorption spectrometers, low-temperature equipment, and apparatus for lifetime measurements have been described.[13,14] Raman spectra were acquired with argon ion laser (457.9 nm) excitation.[15] MM2 calculations were performed on a Tectronics CACHE system.

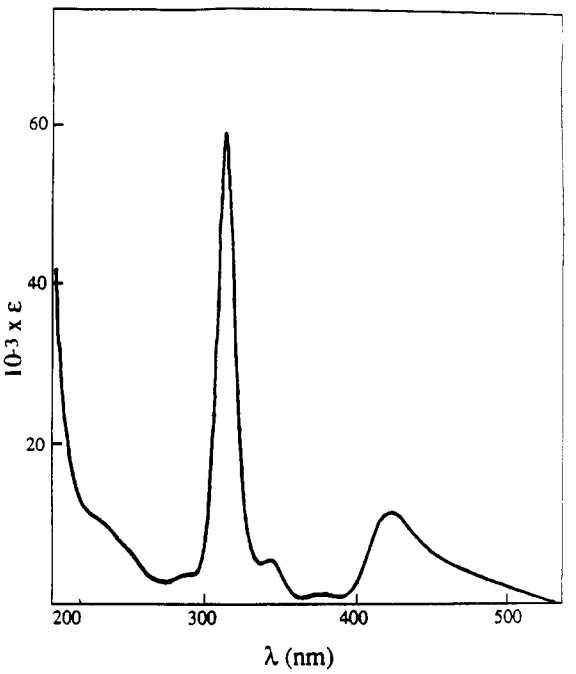

Figure 1. Room-temperature absorption spectrum of $[Rh_2(dimen)_4][PF_6]_2$ (10^{-5} M) in CH_3CN.

Results and Discussion

Electronic Absorption Spectra. The room-temperature solution spectrum of $Rh_2(dimen)_4^{2+}$ (Figure 1) is independent of solvent and anion. The intense band at 314 nm, present in the spectra of all Rh(I) isocyanide complexes,[1-3] is assigned to the $^1(d_{xz,yz} \rightarrow$

(6) Boyd, D. C.; Matsch, P. A.; Mixa, M. M.; Mann, K. R. *Inorg. Chem.* **1986**, *25*, 3331–3333.
(7) (a) Sykes, A. G.; Mann, K. R. *J. Am. Chem. Soc.* **1990**, *112*, 7247–7254. (b) Sykes, A. G.; Mann, K. R. *Inorg. Chem.* **1990**, *29*, 4449–4453. (c) Sykes, A.; Mann, K. R. *J. Am. Chem. Soc.* **1988**, *110*, 8252–8253.
(8) Miskowski, V. M.; Smith, T. P.; Loehr, T. M.; Gray, H. B. *J. Am. Chem. Soc.* **1985**, *107*, 7925–7934.
(9) An X-ray structure analysis of $[Rh_2(dimen)_4Br_2][PF_6]_2$ revealed a Rh–Rh distance of 2.9 Å (Rhodes, M.; Mann, K. R. Unpublished work). The dimen ligands could not be located (reflecting extensive ligand disorder and/or twinning). $[Rh_2(dimen)_4Br_2]^{2+}$ exhibits its $d\sigma \rightarrow d\sigma^*$ transition at 368 nm (ϵ 55 500 M^{-1} cm^{-1}, CH_3CN solution), to be compared to 360 nm (ϵ 60 000 M^{-1} cm^{-1}) for $[Rh_2(TMB)_4Br_2]^{2+}$.
(10) Hill, M. G.; Lamanna, W.; Mann, K. R. *Inorg. Chem.* **1991**, *30*, 4687.
(11) Rice, S. F. Ph.D. Thesis, California Institute of Technology, 1982.
(12) Large bond distortions have been seen for excited van der Waal molecules such as Hg_2: (a) Celestino, K. C.; Ermler, W. C. *J. Chem. Phys.* **1984**, *81*, 1872–1881. (b) Van Zee, R. D.; Blankespoor, S. C.; Zwier, T. S. *J. Chem. Phys.* **1988**, *88*, 4650–4654.
(13) Miskowski, V. M.; Gray, H. B.; Hopkins, M. D. *Inorg. Chem.* **1992**, *31*, 2085–2091.
(14) (a) Rice, S. F.; Gray, H. B. *J. Am. Chem. Soc.* **1983**, *105*, 4571–4575. (b) Milder, S. J.; Brunschwig, B. S. *J. Phys. Chem.* **1992**, *96*, 2189–2196. (c) Nocera, D. G.; Winkler, J. R.; Yocom, K. M.; Bordignon, E.; Gray, H. B. *J. Am. Chem. Soc.* **1984**, *106*, 5145–5150.
(15) Dallinger, R. F.; Miskowski, V. M.; Gray, H. B.; Woodruff, W. H. *J. Am. Chem. Soc.* **1981**, *103*, 1595–1596.

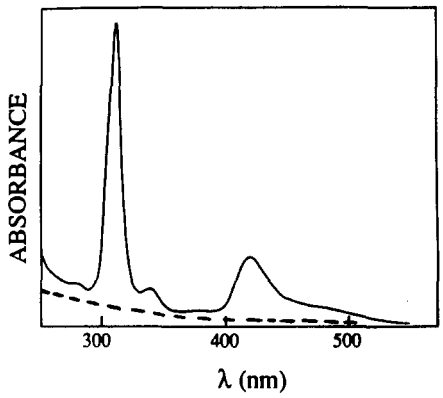

Figure 2. Absorption spectrum of $[Rh_2(dimen)_4][PF_6]_2$ in 3:1 2-MeTHF:CH_3CN glassy solution at 77 K. The dashed line represents the solvent background absorption.

pσ) excitation. Likewise, shoulders at 290 and 342 nm are attributable[3,16] to $^1(d_{xz,yz} \rightarrow p\sigma)$ plus one quantum of ν(CN) and to $^3(d_{xz,yz} \rightarrow p\sigma)$, respectively.[17] These features are negligibly perturbed from the corresponding band energies and intensities of mononuclear complexes, which additionally display strong singlet (~380 nm) and much weaker triplet (~440 nm) $d_{z^2} \rightarrow p_z$ excitations.[1-3] Given that the lowest energy singlet $d_{z^2} \rightarrow p_z$ excitation of d^8–d^8 complexes ($d\sigma^* \rightarrow p\sigma$) is usually strongly red-shifted from the corresponding monomer transition, we assign the 423-nm band of $Rh_2(dimen)_4^{2+}$ (Figure 1) to this excitation. The 423-nm absorption band has a sloping tail at about 480 nm. Although the energy difference between this shoulder and the 423-nm maximum is similar to singlet–triplet splittings of 2500-3000 cm^{-1} previously determined for both binuclear and mononuclear Rh(I) isocyanide complexes, the intensity of the 480-nm shoulder relative to the 423-nm maximum is much greater than is generally seen for the triplet $d_{z^2} \rightarrow p_z$ excitation, even in binuclear iridium(I) complexes[16] that possess stronger spin-orbit coupling.

The absorption spectra of rigid, low-temperature glassy solutions (Figure 2) and crystalline solids dispersed in KCl (Figure 3) are quite similar to the room-temperature solution spectrum, as are diffuse reflectance spectra of the solids diluted with $MgSO_4$ (see the supplementary material). Although lowering the temperature sharpens the 423-nm maximum considerably, the ~480-nm feature does not develop into a resolved band maximum under any conditions. We attribute the temperature dependence of the absorption spectrum to thermal line broadening. Careful Gaussian deconvolution of the low-temperature isotropic spectrum gives two bands centered near 425 and 485 nm with half-widths of ~2000 cm^{-1}. The apparent peak extinction coefficient of the lower energy band is ~5000 M^{-1} cm^{-1}. For the solid-state spectra, the energy of the maximum absorbance varies slightly for the different salts (λ_{max}: 420 nm, PF_6^-; 428 nm, $TFPB^-$; 437 nm, $B(C_6H_5)_4^-$); however, the visible differences in color of these salts (yellow, PF_6^-; orange, $TFPB^-$; red-orange, $B(C_6H_5)_4^-$) are caused by an increase in intensity of the ~480-nm shoulder as a function of decreasing Rh–Rh distance.

Polarized single-crystal spectra for the tetraphenylborate salt of $Rh_2(dimen)_4^{2+}$ at 20 K (Figure 4) were measured for light polarized parallel to each of the two extinctions of the well-developed crystal face ((001) of the orthorhombic space group *Pbca*). The molecular orientations in the crystal are known.[4b] Thus, in the "oriented gas" approximation (assuming effective D_4 symmetry for the chromophore), we calculate that a molecular *z*-polarized transition should display relative intensities in the

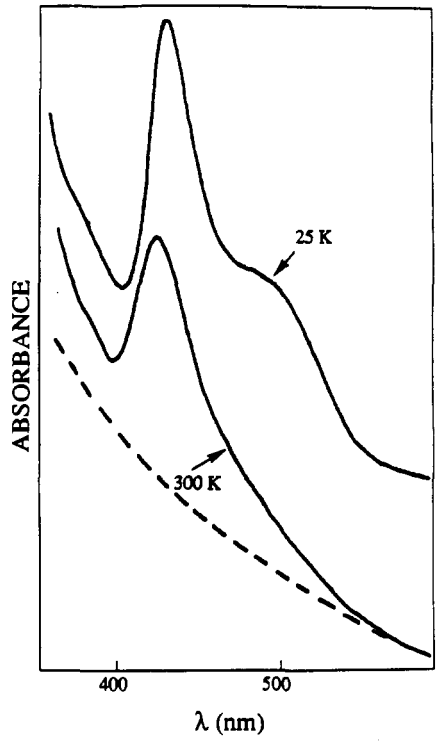

Figure 3. Absorption spectra of $[Rh_2(dimen)_4][O_3SCF_3]_2$ in a KCl disk at room temperature and 25 K. The dashed line shows the interpolated scattering baseline.

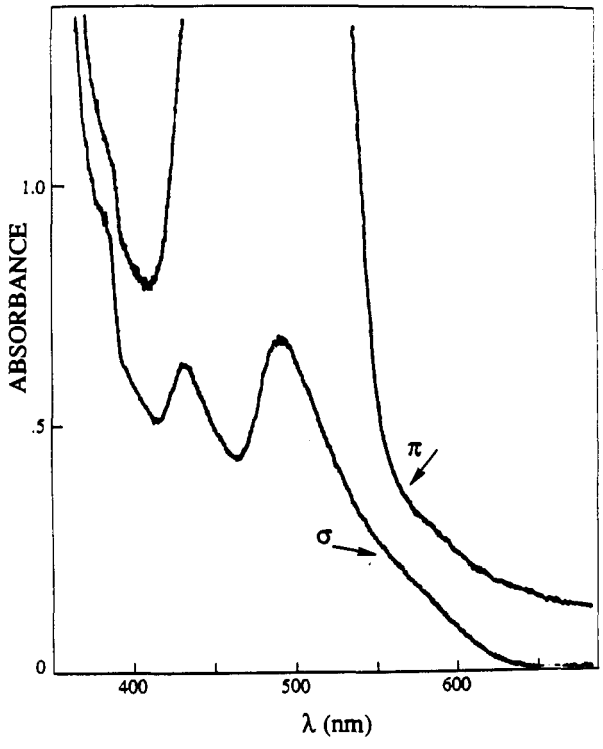

Figure 4. Single-crystal polarized absorption spectrum for $[Rh_2(dimen)_4][B(C_6H_5)_4]_2$ at 20 K. The π spectrum is vertically offset from the σ spectrum by 0.13 absorbance unit. The crystal thickness was about 50 μm.

π(‖*a*) and σ(‖*b*) polarizations of 0.901 and 0.092, respectively. An *x*,*y*-polarized transition should show intensities of 0.092 and 0.990 for π and σ polarizations. (Intensities here are defined such that the total intensities parallel to the *a*, *b*, and *c* axes sum to 1.0 and 2.0 for *z*- and *x*,*y*-polarized transitions, respectively.) Thus, the σ and π spectra are nearly pure molecular *x*,*y* and *z* spectra and will henceforth be described as "*x*,*y*"- or "*z*"-polarized. For the *z* extinction (Figure 4), the absorbance in the 430-550-

(16) Smith, D. C.; Mason, W. R.; Miskowski, V. M.; Gray, H. B. *J. Am. Chem. Soc.* **1990**, *112*, 3759-3767.

(17) The 290-nm feature could alternatively be assigned to a spin-forbidden transition of the type $^3(d_{xy} \rightarrow p_z)$. See: Geoffroy, G. L.; Isci, H.; Litrenti, J.; Mason, W. R. *Inorg. Chem.* **1977**, *16*, 1950-1955. The assignments of features in this region have been discussed in detail.[16]

nm region is too intense to measure even for the thinnest crystals available, but two maxima (432 and 490 nm) and a shoulder at ~575 nm are apparent in the (x,y) spectrum.

It is clear from comparison to the isotropic spectra (Figures 1–3) that the ~423- and ~480-nm features are molecular z-polarized. As the spin-forbidden $^3(d\sigma^* \rightarrow p\sigma)$ transition is dipole-allowed only in the x,y direction via the $E_u(^3A_{2u})$ (D_{4h} labels) spin–orbit component,[1-3] *the ~480-nm shoulder cannot be the triplet transition.* Figure 4, however, reveals a likely candidate for the spin-forbidden excitation, namely the 490-nm maximum and its 575-nm shoulder in the x,y polarization. Both the relative weakness of the 490-nm band and its 2750-cm^{-1} splitting from the 423-nm maximum are characteristics of a $^3(d\sigma^* \rightarrow p\sigma)$ excitation.[1-3] Furthermore, the ~575-nm shoulder has the same relative relationship to the 490-nm maximum in x,y polarization as the 480-nm shoulder does to the 423-nm maximum of the isotropic spectra. We propose that these x,y-polarized features (490-nm maximum, 575-nm shoulder) are the spin-forbidden analogues of the intense spin-allowed features.

Raman Spectra. Binuclear Rh(I) complexes display resonance enhancement of the $\nu(Rh_2)$ Raman band and its overtones with excitation into the $^1A_{1g} \rightarrow {}^1A_{2u}$ electronic transition.[15] This enhancement results from the large distortion along the Rh–Rh axis upon excitation from the ground to the excited state.[1-3] A time-resolved resonance Raman study of $Rh_2b_4^{2+}$ in CH_3CN[15] has established that $\nu(Rh_2)$ is 79 cm^{-1} in the ground state and 144 cm^{-1} in the $^3(d\sigma^* \rightarrow p\sigma)$ excited state; the corresponding $Rh_2(TMB)_4^{2+}$ frequencies are 55 and 151 cm^{-1}.[15] For $Rh_2b_4^{2+}$, the frequency increase indicates that the excited-state bond contraction is ~0.23 Å. The only other vibrational modes that display any perceptible intensity enhancement in resonance with the $^1A_{1g} \rightarrow {}^1A_{2u}$ transition for either binuclear or mononuclear Rh(I) isocyanide complexes are ν(Rh–C) and ν(CN); in both of these cases the enhancement is very small.[15,18,19]

The resonance Raman spectrum (457.9-nm excitation) of $Rh_2(dimen)_4^{2+}$ in CH_3CN shows a band at 28 cm^{-1} and an overtone at approximately 56 cm^{-1}, in addition to the intense Rayleigh background scattering of CH_3CN (Figure 5). (The 28-cm^{-1} line was also observed in the anti-Stokes spectrum.) We assign the 28-cm^{-1} feature to $\nu(Rh_2)$, because it follows the general metal–metal bond length/frequency correlation observed for other bridged Rh(I) dimers and compares favorably with the observed stretching frequencies of van der Waals molecules such as Xe_2 (r_e = 4.36 Å, $\nu(Xe_2)$ = 21 cm^{-1}).[20]

We believe that the normal mode corresponding to this band contains a significant component of ligand deformation. Because the bridging ligands impose the long Rh–Rh distance in $Rh_2(dimen)_4^{2+}$, they must also contribute to the restoring force for the vibration along the metal–metal coordinate. This mode is strongly enhanced by excitation in the visible region. By analogy to other binuclear Rh(I) complexes, we infer that there must be a large reduction of the Rh–Rh bond length in the enhancing excited state, which we assign to $^1A_{2u}$ (in D_{4h} symmetry). We expect a significant increase in the frequency of this normal mode in the $^1A_{2u}$ and $^3A_{2u}$ excited states, but because of their subnanosecond lifetimes, we have not been able to measure these stretches in fluid solutions.

Electronic Emission Spectra. The room-temperature and 77 K electronic emission spectra for $Rh_2(dimen)_4^{2+}$ in 2-MeTHF/CH_3CN are shown in Figure 6. The relevant photophysical parameters are summarized in Tables 1–3, together with some

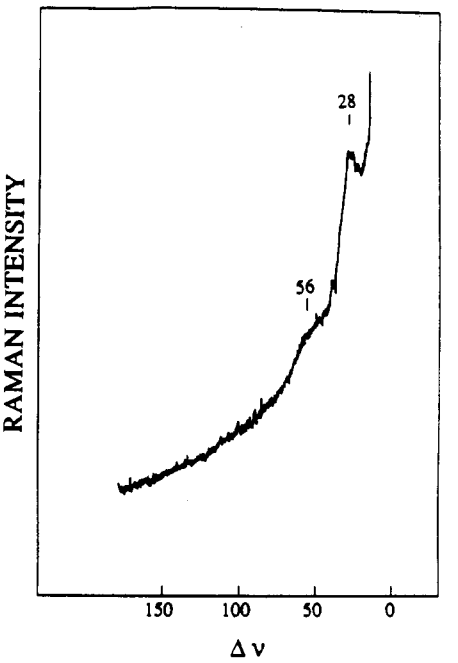

Figure 5. Raman spectrum of $[Rh_2(dimen)_4][PF_6]_2$ in CH_3CN using 457.9-nm excitation.

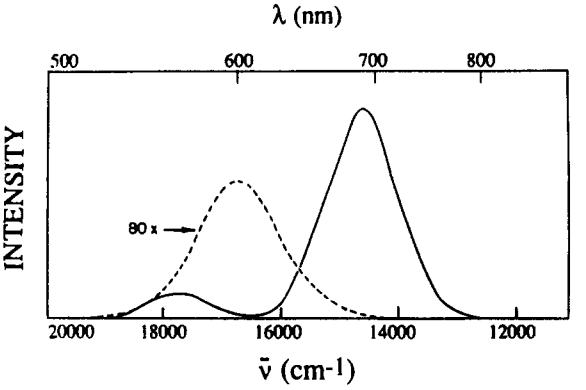

Figure 6. Corrected emission spectra (436-nm excitation) of $[Rh_2(dimen)_4][PF_6]_2$ in 3:1 2-MeTHF:CH_3CN solution at room temperature (- - -) and 77 K (—).

Table 1. Corrected Emission Maxima (nm) for $Rh_2(dimen)_4^{2+}$ in Various Media

	fluorescence		phosphorescence	
solvent	300 K	77 K	300 K	77 K
3:1 2-MeTHF:CH_3CN soln	600	562	*a*	690
1:1 CH_3OH:C_2H_5OH soln[b]	591	560	*a*	680
PMMA film	573	565	690 sh	700
PF_6^- salt[c]	550	545	660 sh	665
$TFPB^-$ salt[c]	562	560	*a*	682
$B(C_6H_5)_4^-$ salt[c]	587	588	700 sh	714

[a] Not observed. [b] At 165 K, the fluorescence and phosphorescence maxima in this solvent are 595 and 735 nm, respectively. [c] Crystalline solid.

$Rh_2(TMB)_4^{2+}$ data[1] for comparison. Both the dimen and TMB complexes show a fluorescence band and a dramatically temperature-dependent phosphorescence band (*vide infra*). The fact that emission can be observed at all from $Rh_2(dimen)_4^{2+}$ in fluid solution sharply differentiates this complex from mononuclear Rh(I) compounds;[21] the additional observation that the emissions are red-shifted from mononuclear emission[2,21] suggests that the emissive excited states are more strongly metal–metal bound than the ground states. The fluorescence intensity of $Rh_2(dimen)_4^{2+}$

(18) Carlson, M.; Dallinger, R. F. Unpublished work.
(19) The absence of significant CN distortion in the $^3A_{2u}$ excited state of $Rh_2b_4^{2+}$ has been confirmed by transient IR studies: Doorn, S. K.; Gordon, K. C.; Dyer, R. B.; Woodruff, W. H. *Inorg. Chem.* **1992**, *31*, 2284–2285.
(20) Huber, K. P.; Herzberg, G. *Molecular Spectra and Molecular Structure*; Van Nostrand: Princeton, NJ, 1979; Vol. IV, Constants of Diatomic Molecules.
(21) Andrews, L. J. *J. Phys. Chem.* **1979**, *83*, 3203–3209.

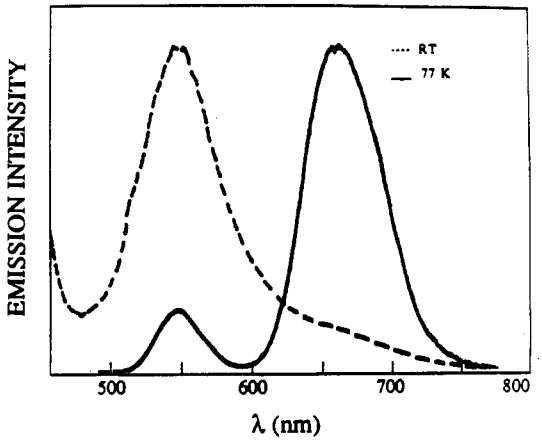

Figure 7. Corrected emission spectra (440-nm excitation) of solid $[Rh_2(dimen)_4][PF_6]_2$ at room temperature (- - -) and 77 K (—). The rising signal below 500 nm in the room-temperature spectrum is due to scattered light. Emission intensities are normalized.

Table 2. Photophysical Parameters for $Rh_2(TMB)_4^{2+}$ and $Rh_2(dimen)_4^{2+}$ [a]

	295K				77K			
	τ_F (ns)	Φ_F	τ_P (ns)	Φ_P	τ_F (ns)	Φ_F	τ_P (μs)	Φ_P
TMB	0.9[b]	0.055	30	$\sim 10^{-3}$ [c]	1.4[d]	0.09	20.5	0.52
dimen	0.23[d]	0.0016[e]	<1[f]	$<10^{-4}$	1.5[d]	0.016	21.0	0.17

[a] Unless otherwise indicated, the solvent is a 3:1 2-MeTHF:CH_3CN solution. Lifetime values were determined by luminescence decay. The TMB data have been previously reported.[1] [c] Poorly resolved from the intense fluorescence. [d] PMMA film. [e] For 436-nm excitation; this value is larger by a factor of 2 for 500-nm excitation; see Figure 9. [f] Upper limit determined by the absence of transient absorption on this time scale.

Table 3. Radiative and Nonradiative Rate Constants (s^{-1})[a] for $Rh_2(TMB)_4^{2+}$ and $Rh_2(dimen)_4^{2+}$

		fluorescence		phosphorescence	
		TMB	dimen	TMB	dimen
295 K	k_f	6×10^7	1×10^7 [b]	$\sim 4 \times 10^4$	c
	k_{nr}	1×10^9	4×10^9	3×10^7	$>5 \times 10^8$
77 K	k_f	6×10^7	1×10^7	2.7×10^4	8×10^3
	k_{nr}	6×10^8	7×10^8	2.2×10^4	4×10^4

[a] Derived from data in 1. [b] Using the 500-nm quantum yield. [c] Not estimated.

is more temperature sensitive than that of the other binuclear Rh(I) complexes that we have examined.[1] The very large shift in λ_{max} for $Rh_2(dimen)_4^{2+}$ fluorescence between room and low temperature shown in Figure 6 also differentiates $Rh_2(dimen)_4^{2+}$ from other d^8–d^8 systems: $Rh_2(TMB)_4^{2+}$, for example, shows only a 2-nm shift of its fluorescence maximum under similar conditions.

The 77 K solid-state emissions of the crystalline PF_6^- (Figure 7), $TFPB^-$, and $B(C_6H_5)_4^-$ salts (as well as PMMA films) are all similar to the 77 K glassy solution emissions, and the room-temperature emissions are all similarly weak. However, the solid-state spectra differ from the solution spectra in that fluorescence maxima are nearly temperature-independent.

When the temperature of an ethanol glass of $[Rh_2(dimen)_4][PF_6]_2$ is raised from 77 to 150 K (just below the softening point of the glass), both emission bands broaden slightly and red-shift by ~3 nm (~100 cm^{-1}). There is no change in the integrated fluorescence intensity over this temperature range, but a thermally activated nonradiative decay process reduces the phosphorescence intensity observed at 150 K to about one-third of that observed at 77 K. When the temperature is raised to 165 K (a temperature above the glass/fluid transition of ethanol), both emissions

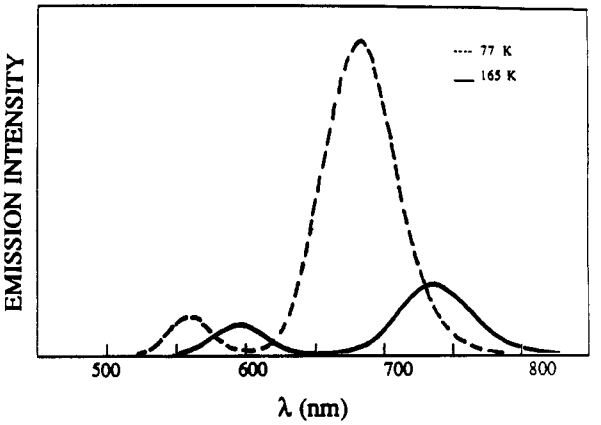

Figure 8. Corrected emission spectra (440-nm excitation) of $[Rh_2(dimen)_4][PF_6]_2$ in C_2H_5OH at the indicated temperatures.

abruptly red-shift by ~1000 cm^{-1} (Figure 8), and a fluorescence maximum similar to the room-temperature value is observed (Table 1). This shift occurs within a 10 K temperature range.

These properties are symptomatic of rigidochromism, as observed for several mononuclear Rh(I)[21] and Ru(II)[22] complexes. Whereas the previous cases showed dramatic changes in emission yields and lifetimes as the glassy matrix softened, we see only small effects on these parameters for $Rh_2(dimen)_4^{2+}$. A likely explanation for our observations is that the rigid matrix suppresses certain types of distortions of the bulky dimen ligands.

The 77 K emission maxima for the solid $TFPB^-$ salt are in close agreement with those in glassy matrices; the corresponding maxima for the solid PF_6^- compound are blue-shifted by about 500 cm^{-1}. Given that the Rh–Rh distance for $[Rh_2(dimen)_4][PF_6]_2$ is substantially (0.23 Å) longer than that for $[Rh_2(dimen)_4][TFPB]_2$, our results suggest that the bond distance in the latter compound (4.246 Å) may be closer to the average distance in solution. Interestingly, the emission maxima for the crystalline $B(C_6H_5)_4^-$ compound are close to those observed for *fluid* solutions, even though the solid-state absorption maxima of the other salts match those of fluid solutions better than those of the $B(C_6H_5)_4^-$ material. It is likely that the excited chromophore adjusts its torsional angle prior to emission in fluid solution, whereas in a crystal it probably cannot. Thus, we suggest that the average ground-state Rh–Rh bond length in solution will be similar to those of the $TFPB^-$ and PF_6^- salts, whereas the average twist angle of the relaxed excited state may be closer to the ~16° torsional angle of the $B(C_6H_5)_4^-$ compound.

The temperature-dependent phosphorescence lifetime data (532-nm excitation) in 3:1 2-MeTHF:CH_3CN solution were fit to eq 2 (k_B is the Boltzmann constant), with $k_0 = 4.9 \times 10^4$ s^{-1},

$$k = k_0 + A \exp(E_a/k_B T) \qquad (2)$$

$E_a = 2610$ cm^{-1}, and $A = 5 \times 10^{14}$ s^{-1} (the extrapolated room-temperature triplet lifetime is 500 ps). The temperature dependence of the fluorescence lifetime was also determined (Figure 9) for a sample dissolved in PMMA, again with 532-nm excitation. The data were fit to eq 2 with values of $k_0 = 6.8 \times 10^8$ s^{-1}, $E_a = 1030$ cm^{-1}, and $A = 6 \times 10^{11}$ s^{-1}. The activation energies for both $^3A_{2u}$ and $^1A_{2u}$ nonradiative decays of $Rh_2(dimen)_4^{2+}$ are very similar to those previously found for $Rh_2(TMB)_4^{2+}$,[1,23] but the A terms are about 1 order of magnitude larger.

(22) Kitamura, N.; Sato, M.; Kim, H.-B.; Obata, R.; Tazuke, S. *Inorg. Chem.* **1988**, *27*, 651–658.
(23) (a) Milder, S. J. *Inorg. Chem.* **1985**, *24*, 3376–3378. (b) Rice, S. F.; Milder, S. J.; Gray, H. B.; Goldbeck, R. A.; Kliger, D. S. *Coord. Chem. Rev.* **1982**, *43*, 349–354.

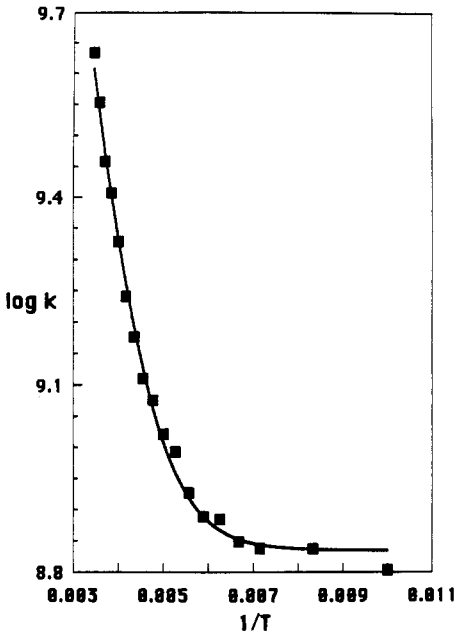

Figure 9. Temperature dependence of the fluorescence lifetime of $[Rh_2(dimen)_4][PF_6]_2$ in 4:1 C_2H_5OH:CH_3OH solution.

Radiative and nonradiative rate constants for $Rh_2(TMB)_4^{2+}$ and $Rh_2(dimen)_4^{2+}$ are given in Table 2; the k_r values for the dimen complex are lower than the TMB values by factors of about 6 (fluorescence) and 3 (phosphorescence). Using the energy of the fluorescence maximum (558 nm) and the ~480-nm shoulder, we calculate $k_r = 1.5 \times 10^7$ s^{-1} (Strickler–Berg method[24]), in good agreement with the experimental value (Table 2). Similarly good agreement has been found between experimental and Strickler–Berg k_r values for the fluorescence and phosphorescence of other binuclear Rh(I) complexes.[1-3,25]

Emission Excitation Spectra. In the absence of wavelength-dependent excited-state decay processes, the corrected room-temperature fluorescence excitation spectrum (Figure 10) would be equivalent to the absorption spectrum. The 317-nm feature is very intense in absorption (Figure 1) but appears only weakly in the excitation spectrum. This pattern has been observed in the fluorescence excitation spectra of other binuclear rhodium(I) complexes;[1] it implies that there is direct decay of the upper excited states to the $^3(d\sigma^* \rightarrow p\sigma)$ state.

Fluorescence excitation spectra of other binuclear d^8–d^8 complexes show upper state absorptions with decreased intensity, but with little or no change in band shape relative to the ground state; the $^1(d\sigma^* \rightarrow p\sigma)$ quantum yields for nonradiative decay are independent of excitation energy within a given band.[1] In contrast, the fluorescence yield for $Rh_2(dimen)_4^{2+}$ (Figure 10) decreases rapidly with increasing excitation energy within the ~425-nm absorption system.

The polarized fluorescence excitation spectrum of $Rh_2(dimen)_4^{2+}$ in an ethanol glass at 77 K is presented in Figure 11a, while Figure 11b gives the polarization ratio N ($=I_\parallel/I_\perp$) as a function of wavelength. Although the $^1(d_{xz,yz} \rightarrow p_z)$ excited state gives a low fluorescence yield at 77 K, the 77 K excitation spectrum in the 400–530-nm region is in much closer agreement with the corresponding absorption spectrum (Figure 2) than is observed at room temperature. The three possible theoretical values for polarization ratios of a uniaxial chromophore are as follows:[26] 3, if both the emission and absorption are polarized along the unique z axis; $^4/_3$, if both emission and absorption are polarized perpendicular to z; and $^1/_2$, if emission and absorption are polarized parallel and perpendicular, respectively, to z (or *vice versa*). In practice, sample imperfections always result in some loss of polarization.[1,13] For the three listed cases, our apparatus gives experimental values of 1.9–2.4, ~1.25, and ~0.6, respectively, for numerous test molecules.

Figure 10. Corrected fluorescence excitation spectrum (monitored at 605 nm) for $[Rh_2(dimen)_4][PF_6]_2$ in C_2H_5OH at room temperature. The dashed line shows part of the absorption spectrum, which has been normalized to the excitation spectrum at 500 nm.

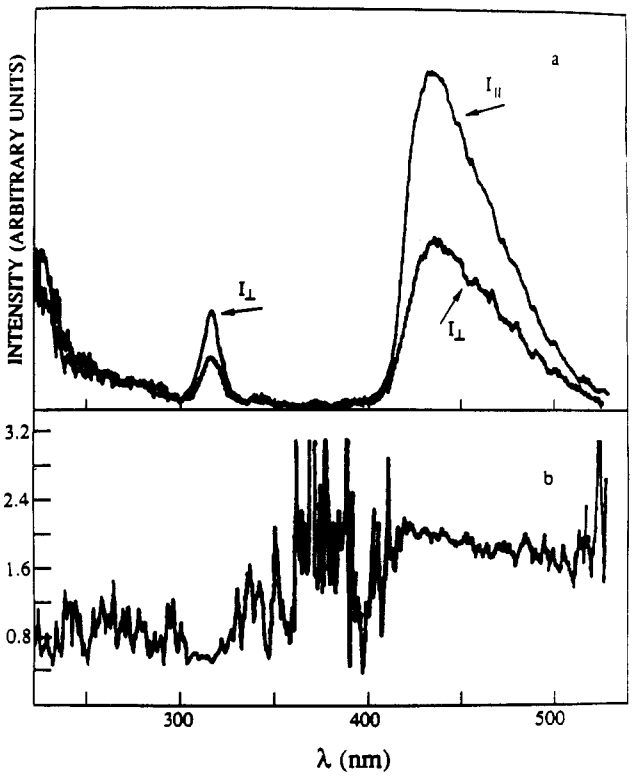

Figure 11. (a) Polarized fluorescence excitation spectrum (monitored at 560 nm) for $[Rh_2(dimen)_4][PF_6]_2$ in a glassy C_2H_5OH solution at 77 K. (b) Polarization ratio N from data of part a.

(24) Strickler, S. J.; Berg, R. A. *J. Chem. Phys.* **1962**, *37*, 814–822.
(25) Milder, S. J.; Kliger, D. S. *J. Phys. Chem.* **1985**, *89*, 4170–4171.
(26) Lakowicz, J. R. *Principles of Fluorescence Spectroscopy*; Plenum Press: New York, 1983.

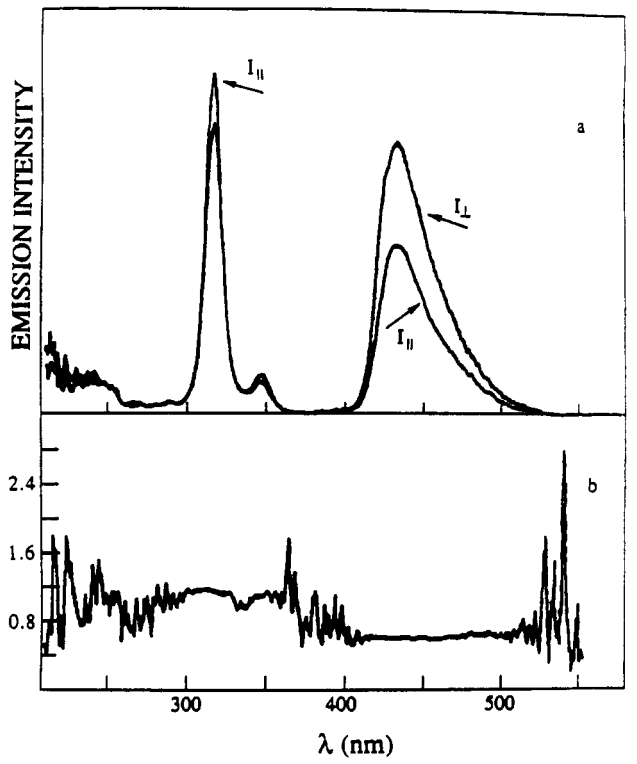

Figure 12. (a) Polarized phosphorescence excitation spectrum (monitored at 679 nm) for $[Rh_2(dimen)_4][PF_6]_2$ in a glassy C_2H_5OH solution at 77 K. (b) Polarization ratio N from data of part a.

The high polarization ratio observed in the 400–530-nm region is uniquely consistent with z-polarized fluorescence, as is expected for a $^1(d\sigma^* \rightarrow p\sigma)$ ($^1A_{2u}$ in D_{4h} symmetry) excited state. The polarization ratio for the 317-nm feature is indicative of an x,y-polarized absorption, consistent with assignments[1-3,16] of the analogous band in related complexes to $^1(d_{xz,yz} \rightarrow p\sigma)$ (the excited state is ^1E_u in D_{4h} symmetry).

The phosphorescence excitation polarization ratios (Figure 12) are consistent with x,y-polarized emission from the $^3(d\sigma^* \rightarrow p\sigma)$ [$E_u(^3A_{2u})$] excited state. It is striking that the entire absorption region from 400 to 530 nm is z-polarized, in accord with our single-crystal absorption data. The transitions to the ^1E_u and $E_u(^3E_u)$ ($d_{xz,yz} \rightarrow p_z$) excited states are each much weaker (Figure 12) relative to the 400–530-nm absorption than they are in the absorption spectrum (Figures 1 and 2). In contrast, other binuclear Rh(I) compounds[1] show phosphorescence excitation spectra that agree well with absorption spectra. The unique behavior of $Rh_2(dimen)_4^{2+}$ implies that a significant amount of upper excited-state excitation decays via a nonradiative route that bypasses the phosphorescent $^3(d\sigma^* \rightarrow p\sigma)$ excited state, most likely proceeding directly to the ground state.

Assignments of the Visible Absorptions. The spectroscopic data suggest that the ~480-nm shoulder (isotropic spectrum, Figure 1) and the weak ~575-nm shoulder (x,y-polarized single-crystal spectrum, Figure 4) must correspond to transitions to relatively strongly metal–metal-bound $(d\sigma^* \rightarrow p\sigma)$ $^1A_{2u}$ and $E_u(^3A_{2u})$ excited states, since these are the absorption features that have a "mirror-image" relationship to the strong low-temperature emissions that characterize a metal–metal-bound excited state.[1-3,14b] It is likely, then, that the 425- and 490-nm absorption maxima represent another singlet/triplet pair of excited states. Our data show that the 425- and 490-nm bands are z- and x,y-polarized, respectively, and that the corresponding excited states are stabilized with respect to any known monomer excited state.[1-3]

The only excited states of either mononuclear or binuclear Rh(I) isocyanide complexes that have been spectroscopically identified at wavelengths greater than 250 nm are formed by d $\rightarrow p_z$ transitions.[1-3] In D_4 (or D_{4h}) symmetry, the only spin- and z-dipole-allowed transitions arise from $d_{z^2} \rightarrow p_z$ excitations. In the MO formalism,[1-3] there are four binuclear one-electron d_{z^2} excitations, yielding two A_1 and two A_2 excited states. One of the A_2 states is the $d\sigma^* \rightarrow p\sigma$ excitation that has already been extensively discussed. However, an assignment of the 425-nm absorption as a transition to the other $^1A_2$ excited state is not reasonable. In the MO picture, this excited state is very strongly metal–metal antibonding ($d\sigma \rightarrow p\sigma^*$); thus it cannot fall below the ~380-nm monomer $d_{z^2} \rightarrow p_z$ state.

We have shown previously that a valence-bond (VB) model can account for the spectroscopic properties of weakly metal–metal-bonded d^8–d^8 complexes.[16] In the VB picture, the monomer excitation undergoes Davydov[27] coupling in the dimer to give A_{1g} and A_{2u} (D_{4h} symmetry) excited states. The A_{2u} state corresponds to the $^1(d\sigma^* \rightarrow p\sigma)$ MO excitation, while the A_{1g} state is expected[16] to be essentially unperturbed from the monomer. Indeed, d^8–d^8 systems show[3,16] weak transitions very near the intense transitions found in monomers $(Rh_2(dimen)_4^{2+}$ exhibits such a weak feature near 380 nm; Figures 1, 2, and 4).

The other states in the VB picture are an A_{1g}, A_{2u} pair corresponding to the metal-to-metal charge transfer. These states should be strongly destabilized relative to monomer excited states, even in the absence of metal–metal bonding. On the basis of theoretical estimates of the destabilization, we have tentatively assigned the lowest metal-to-metal charge-transfer (MMCT) excitations to broad absorptions at wavelengths less than 250 nm for several d^8–d^8 compounds.[16] $Rh_2(dimen)_4^{2+}$ has similar absorptions in this region (Figure 1), thereby indicating that its MMCT excitations are at these energies or higher.

Thus, d $\rightarrow$ p excitations do *not* give two z-polarized singlet–singlet absorptions lower than the monomer transitions, so an alternative assignment of the 425-nm feature must be considered. One possibility is that the potential energy surface of the $^1A_{2u}$ $(d\sigma^* \rightarrow p\sigma)$ excited state intersects with (and is strongly perturbed by) a ligand-field excited state. The entire ~400-550 nm-absorption envelope might then be due to the $^1A_{1g} \rightarrow {}^1A_{2u}$ $(d\sigma^* \rightarrow p\sigma)$ transition, which would explain the uniform z polarization. In this model, possible perturbing states could involve $d_{x^2-y^2}$ population. Although we cannot rule out this possibility, we prefer a similar explanation that does not invoke a second excited state. Specifically, we propose that the asymmetric visible absorption of $Rh_2(dimen)_4^{2+}$ results from an extremely anharmonic $d\sigma^* \rightarrow p\sigma$ excited-state potential surface, which minimizes at a Rh–Rh distance dramatically shorter than the ground-state equilibrium separation. The basis of this explanation is the repulsive ligand potential inferred from the $[Rh_2(dimen)_4][Y]_2$ crystal structures (Y = PF_6, TFPB, $B(C_6H_5)_4$).[4]

Description of the Potential Surfaces. To obtain semiquantitative information about the effect of ligand conformation on the relevant potential surfaces, we have carried out MM2 calculations on an isolated dimen ligand (with "dummy" metal atoms). As the metal–metal bridging distance is varied from 5.5 to 2.5 Å, dimen exhibits a very shallow energy minimum at 5.0 Å. This minimum lies between the 5.28-Å Ir–Ir separation in $[AgIr_2(dimen)_4(DMSO)_2][PF_6]_2$[7c] and the 3.861-Å Rh–Rh distance in $[Rh_2(dimen)_4][B(C_6H_5)_4]_2$.[4b] At each point along this metal–metal coordinate, the dimen ligand minimizes to a geometry in which the two CN groups are perfectly eclipsed. This result agrees with predictions based on the crystal structures of $[AgIr_2(dimen)_4(DMSO)_2][PF_6]_3$[7c] and $[Rh_2(dimen)_4][TFPB]_2$,[4b] in which the individual metal centers undergo local C_{4v} distortions along the square planar a_{2u} out-of-plane bending coordinate to accommodate an eclipsed arrangement of dimen ligands.

In Figure 13 we show the effect of this MM2 ligand potential on the calculated $^1A_{1g}$ (ground state) and $^3A_{2u}$ surfaces of Rh_2-

(27) Craig, D. P.; Walmsley, S. H. *Excitons in Molecular Crystals*; Benjamin: New York, 1968.

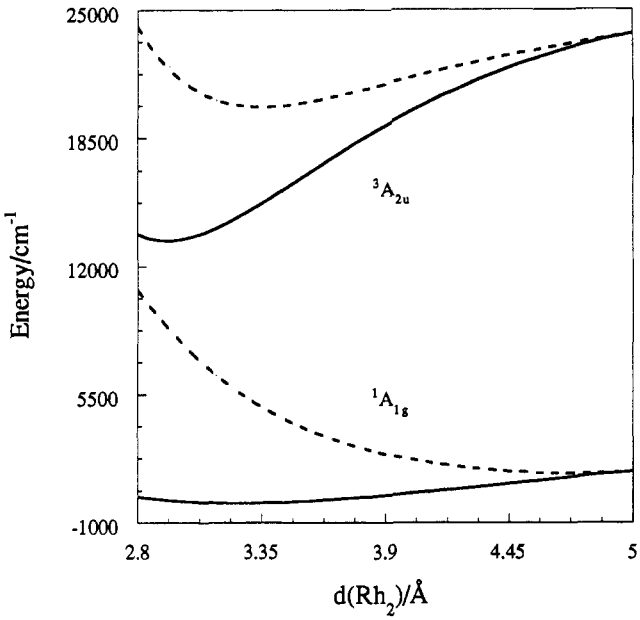

Figure 13. Calculated potential energy surfaces for the $^1A_{1g}$ and $^3A_{2u}$ ($d\sigma^* \rightarrow p\sigma$) states of $Rh_2(dimen)_4^{2+}$. The solid lines are diatomic Morse potentials calculated for respective ground- and excited-state $\nu(Rh_2)$ values of 55 and 151 cm^{-1} (experimental values for $Rh_2(TMB)_4^{2+}$)[15] and dissociation energies of 12 and 36 kcal/mol.[3] The dashed lines are the Morse potentials plus 4 times the calculated MM2 potential for a dimen ligand (see text) referenced to zero at 5.0 Å.

$(dimen)_4^{2+}$ (the $^1A_{2u}$ surface is not shown but should resemble the $^3A_{2u}$ surface destabilized by about 3000 cm^{-1}).[1-3] The solid lines represent Morse potentials calculated for an *unbridged* $Rh_2(CNR)_8^{2+}$ molecule using estimates presented elsewhere for the diatomic force constants,[15,18] bond energies,[3] and $^1A_{1g} \leftrightarrow {}^3A_{2u}$ 0–0 energy difference.[3] Adding 4 times the calculated dimen ligand strain energy to these surfaces yields the dashed curves in Figure 13. The resulting potentials yield a ground-state surface that is dominated by the dimen ligand deformational energy. Thus the extremely broad minimum near 4.75 Å is shifted only slightly from the free-ligand value, and the ground-state surface is nearly harmonic in the range 3.3–5.0 Å.[28] In contrast, the excited-state surface retains a minimum at a relatively short (3.35 Å) metal–metal distance but is extraordinarily anharmonic, flattening out near the ground-state minimum because of the ligand preference for this distance.

These potential energy surfaces account for many of the curious properties of this molecule:

1. The very flat ground-state surface is consistent both with the low observed Raman $\nu(Rh_2)$[28] and with the observed variability in ground-state metal–metal distance as a function of anion; such a shallow minimum should be very susceptible to environmental perturbations (e.g., "crystal packing forces").

2. The vertical $^1A_{1g} \rightarrow {}^3A_{2u}$ and $^3A_{2u}$ (relaxed) $\rightarrow {}^1A_{1g}$ transitions are predicted to occur at 475 and 670 nm, respectively. These values compare well to the observed maxima, at 490 (single-crystal absorption data, Figure 4) and 680-714 nm (77 K emission, Table 1), respectively. Moreover, phosphorescence from the $^3A_{2u}$ state is seen to terminate in a gently varying and nearly harmonic portion of the ground-state surface, so the emission is expected to be broad (there is a very large change in equilibrium Rh–Rh distance) but roughly symmetric, as observed (Figures 7 and 8).

In contrast, vertical *absorption* terminates in an anharmonic region of the $^3A_{2u}$ excited-state surface, the shape of which is dominated by the dimen ligand potential. Thus, in the vicinity of the vertical transition, the $^1A_{1g} \rightarrow {}^3A_{2u}$ band, as well as the $^1A_{1g} \rightarrow {}^1A_{2u}$ absorption, should resemble narrow "monomer-like" $d_{z^2} \rightarrow p_z$ transitions because of the gentle slopes of both ground- and excited-state surfaces. However, the minimum in the excited-state surface lies over 1 Å to shorter Rh–Rh distances. This should produce an asymmetric absorption profile. We attribute the entire ~425-nm peak plus the ~480-nm shoulder in the $Rh_2(dimen)_4^{2+}$ absorption spectrum to the $^1A_{1g} \rightarrow {}^1A_{2u}$ ($^1A_1 \rightarrow {}^1A_2$ in D_4 symmetry) transition; the sharp peak represents the vertical vibronic transitions between the ligand-dominated (long Rh–Rh distances) portions of both surfaces, while the shoulder represents the vibronic transitions to the region of the excited-state surface close to the excited-state minimum. These latter transitions become exceedingly weak near the 0–0 transition, as ΔQ(Rh–Rh) is very large.

3. The anomalously low k_r values for $Rh_2(dimen)_4^{2+}$ (*vide supra*), which we were able to correlate with the intensity of the ~480-nm shoulder, are consistent only with the shoulder portion of the absorption band being relevant to emissive processes.[29] Our observation that in fluid solution the vertical (peaked) absorption does not efficiently yield fluorescence (Figure 10) indicates that the ligand-constrained vertical excited state undergoes rapid nonradiative decay processes other than relaxation to the 0–0 level of the $^3A_{2u}$ state. Very likely, these are similar to the rapid excited-state decay processes (perhaps involving decay through ligand-field type excited states) that have been documented for mononuclear Rh(I) complexes.[21]

4. The vertical absorption and emission maxima of the crystalline $B(C_6H_5)_4^-$ salt are both red-shifted by about 1000 cm^{-1} from those of the crystalline PF_6^- salt. These shifts are substantial but perhaps surprisingly small in view of the 0.62-Å difference in ground-state Rh–Rh separation. They can be understood in terms of Figure 13 as involving shifts of the dimen ligand potential minimum to shorter Rh–Rh distances, owing to small environmental perturbations. The *major* effect of such a shift is to intensify the absorption shoulder as ΔQ between relaxed ground and excited states decreases.

While qualitatively instructive, the above potential surfaces do not quantitatively reproduce the observed absorption profile of $Rh_2(dimen)_4^{2+}$. For example, the low-temperature absorption band shape can be calculated semiclassically by "reflecting" the square of the zeroth ground-state vibrational wave function[28] (a Gaussian) off the excited-state potential surface. Such a calculation based on our surfaces does predict a long-wavelength shoulder, but with less intensity than is observed experimentally (although a slight shift in the excited-state minimum toward a longer Rh–Rh bond would give better agreement).

Moreover, the above calculations do not account for a second mode of dimen ligand deformation that appears to be important at short metal–metal distances: crystal structures for $M_2(dimen)_4^{2+}$ complexes with metal–metal bond lengths less than ~3.9 Å show substantial twists of the dimen ligands along the metal–metal axis. Thus, the square planar $Rh(CN)_4$ units in $[Rh_2(dimen)_4][B(C_6H_5)_4]_2$ (Rh–Rh = 3.861 Å) are staggered at an average dihedral angle of 16.2°;[4b] the analogous $Ir(CN)_4$ units in $[Ir_2(dimen)_4(PPh_3)(AuPPh_3)][PF_6]_3$ (Ir–Ir = 2.986 Å)[7a] are staggered by 39°. Presumably, this twisting occurs to relieve the energy associated with the local C_{4v} distortions at the square planar Rh(I) centers (which necessarily result for an eclipsed arrangement of dimen ligands around a Rh_2 core possessing a

(28) The "Morse plus MM2" potential surfaces of Figure 13 could be fit to harmonic (quadratic) expressions in the vicinity of their energy minima (3.35–5.0 Å for the ground state and 3.0–3.6 Å for the excited state), yielding diatomic force constant/stretching frequency values of 0.029 mdyn Å^{-1}/31 cm^{-1} for the ground state and 0.258 mdyn Å^{-1}/92 cm^{-1} for the $^3A_{2u}$ excited state. The former frequency compares well to our measured (Raman) value of 27 cm^{-1}. The latter frequency has not been determined.

(29) We used the Strickler–Berg theory to reach this conclusion, and since this theory is not strictly applicable to such a grossly anharmonic case, the significance of this conclusion is debatable. If the excited-state surface truly possessed a double well, however, this conclusion would follow naturally, as the observed emission rates refer only to processes involving the metal–metal-bonded excited-state minimum.

short metal–metal separation). On the basis of the out-of-plane bending frequencies of several $M(CN)_4^{2-}$ complexes,[30] we estimate this unfavorable energy term to be as high as 13 kcal/mol per metal center at a Rh–Rh distance of 3.2 Å.[31]

For the complex in a *rigid* environment (crystal or glass), the calculations (Figure 13) that neglect the twisting distortion are probably more valid, as twisting of the bulky dimen ligands should be suppressed in the excited states. In fluid solution, however, the excited states are likely to undergo relaxation via twisting, and this provides an explanation for the rigidochromic emission effects that we observed near the glass transition temperature of solutions. Unfortunately, since the ground state is destabilized by twisting, we cannot relate the emission shifts between fluid and glassy media to excited-state stabilization in any simple way.

Finally, we emphasize that small changes in assumed Rh–Rh potentials could alter the quantitative predictions of Figure 13. Given that literature estimates for the Rh(I)–Rh(I) bond strength are not very precise (12 ± 6 kcal/mol for the ground state[3]), our description is only qualitative. In particular, either or both the ground and excited states could possess double minima[32] for slightly different parameters, which further complicates this multidimensional problem.

Acknowledgment. We thank Bill Schaefer for X-ray work and George Rossman for allowing us access to equipment in his laboratory. Work at the California Institute of Technology and the University of Minnesota was supported by the National Science Foundation. Work at Brookhaven National Laboratory was performed under Contract DE-AC02-76CH00016 with the U.S. Department of Energy and supported by its Division of Chemical Sciences, Office of Basic Energy Sciences.

Supplementary Material Available: Diffuse reflectance spectra of $[Rh_2(dimen)_4][PF_6]_2$, $[Rh_2(dimen)_4][TFPB]_2$, and $[Rh_2(dimen)_4][B(C_6H_5)_4]_2$ (1 page). Ordering information is given on any current masthead page.

(30) (a) Kubas, G. J.; Jones, L. H. *Inorg. Chem.* **1974**, *13*, 2816–2819. (b) Jones, L. J. *Inorganic Vibrational Spectroscopy*; Marcel Dekker: New York, 1971; Vol. 1.

(31) Surprisingly, MM2 calculations on a dimen ligand twisted by 39° with a metal–metal bite of 3.0 Å suggest that $[Ir_2(dimen)_4Au(PPh_3)_3][PF_6]_3$ possesses an *additional* ~27 kcal/mol in ligand strain energy over the analogous eclipsed structure with a similarly short Ir–Ir bond. This additional strain energy must be offset by a relaxation of the $Rh(CN)_4$ out-of-plane distortion energy; from our calculations, we estimate this latter energy to be ~33 kcal/mol, consistent with this supposition. We emphasize, however, that these calculations are not quantitatively reliable; the crystal structures show comparable distortions in both C–M–C and N–C–M angles, and the (poorly established) force constants for these distortions have not been incorporated into our MM2 calculations in a systematic way.

(32) Variable-temperature infrared spectroscopic studies[4b] of solutions of $Rh_2(dimen)_4^{2+}$ show only a single temperature-independent ν(CN), which argues against a double-well ground-state potential surface for this complex.